FULL PAPER

Dalton
www.rsc.org/dalton

On the importance of electronic and steric effects in the migratory CO insertion step of rhodium–diphosphine catalyzed methanol carbonylation †

Elias Daura-Oller, Josep M. Poblet and Carles Bo *
Departament de Química Física i Inorgànica, Universitat Rovira i Virgili, Pl. Imperial Tàrraco, 1, 43005 Tarragona, Spain. E-mail: bo@quimica.urv.es

Received 8th July 2002, Accepted 24th October 2002
First published as an Advance Article on the web 29th November 2002

To provide further insight into electronic and steric factors and to quantify their relative importance, we studied in detail the migratory CO insertion step for $RhMe(CO)I_2(L–L)$ systems (L–L = dppms ($PPh_2CH_2P(S)Ph_2$) or dppe ($PPh_2CH_2CH_2PPh_2$)), Monsanto catalysts and some electronically unsymmetrical diphosphine model systems. The difference in the reaction rates of dppms and dppe has a clear electronic origin that reflects the different properties of sulfide phosphine (π-donor) and phosphine (π-acid) ligands. Molecular orbital calculations clearly show that dppms strongly increases back-bonding to CO and favors the overlap between CO and methyl. Steric effects modulate the barrier, which decreases more for dppe than it does for dppms. For dppms, the electronic contribution that phenyl phosphine substituents make to lower the barrier is greater than that made by purely steric effects. The sulfide phosphine ligand dppms accelerates the carbonyl insertion because of its π-donor capability. For the diphosphine ligands we studied, the energy barrier varied gradually as basicity varied, and the slowest kinetics is shown by the most electron-donating ligand. The basicity dependence is stronger when the phosphine ligand occupies a *trans* position to CO. On the other hand and in unsymmetrical diphosphine complexes, phosphine basicity affects stability and reactivity in opposite ways.

Introduction

Methanol carbonylation to produce acetic acid is one of the most prominent applications of homogeneous catalysis to industrial processes.[1] The original $[Rh(CO)_2I_2]^-$ catalyst developed at the Monsanto laboratory, and studied some years ago by Forster[2,3] was improved by BP Chemicals using the iridium complex, which is industrially employed in the Cativa process. Experimental data on rhodium-catalyzed methanol carbonylation have been reported[4–7] and very recently there have been various theoretical studies on several aspects of the reaction mechanism. In a pioneering study, Ziegler and coworkers[8] investigated the migratory CO insertion reaction process in $[M(CO)_2I_3(CH_3)]^-$ (M = Rh and Ir) by means of static and dynamic DFT calculations and the effects of the solvent and several ligands *trans* to the methyl group. Very recently, and almost simultaneously, Ivanova *et al.*[9] and Kinnunen *et al.*[10–12] have reported computational studies of the full catalytic cycle and characterized most of the intermediates involved in the Monsanto and Cativa processes.

Phosphine ligands generated much interest and several rhodium complexes were synthesized and tested as catalysts. The catalytic performance upon incorporation of monophosphines, PEt_3,[13] diphosphines, $PPh_2CH_2CH_2PPh_2$ (dppe),[14] and mixed bidentate ligands $PPh_2CH_2P(O)Ph_2$ (dppmo),[15] $PPh_2CH_2P(S)Ph_2$ (dppms),[16,17] *S,P*-$SC_2B_{10}H_{10}PPh_2$ ($Cab^{P,S}$)[18] and $PPh_2CH_2P(NPh)Ph_2$ (dppmn)[19] were similar to or better than $[Rh(CO)_2I_2]^-$ used in the Monsanto process. Electronically unsymmetrical diphosphine complexes are more active than the dppe system but less active than the Monsanto catalyst under industrially significant conditions.[20] While the rhodium complexes of P,O-, P,N- and P,S- donor ligands are all reported to be methanol carbonylation catalysts, either the conditions in which they were used were not suitable[21–23] or the catalysts were found to be unstable.[24,25] However, since each ligand introduces specific electronic and steric effects, the influence of phosphine-based ligands at each step of the reaction mechanism is not yet clear.[20] Haynes and coworkers[17] showed that dppms in [Rh(CO)I(dppms)] dramatically affects the rate the of migratory CO insertion step. The oxidative addition step and the migratory insertion step in the reaction of [Rh(CO)I(dppms)] with MeI are faster than with the $[Rh(CO)_2I_2]^-$ system. When comparing the reactivity of the dppms system to that of the dppe system [Rh(CO)I(dppe)], they found even more dramatic results. At 25 °C, migratory insertion is more than 3000 times faster for the dppms system than for the dppe system. X-Ray data for $[MeIr(CO)I_2(dppms)]$ suggested[17] that rate enhancement has a steric origin due to putative close contacts between a phenylphosphine substituent and the methyl group. These data also suggested that electronic effects could not account for the high reactivity of the dppms system because electron-donating ligands, while promoting oxidative addition, actually retard CO insertion.

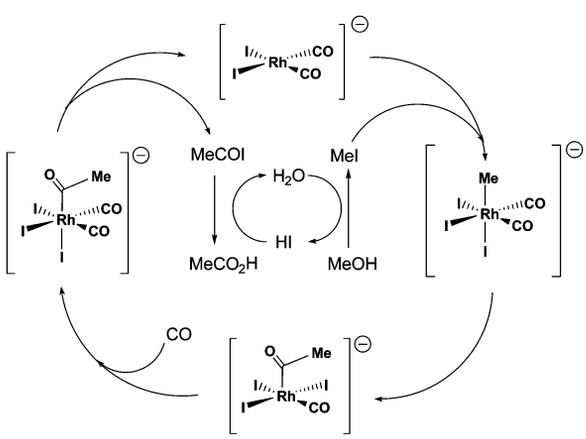

Given that P- and S-donor ligands are electronically different, one would expect the different phosphine– and sulfide–phosphine–rhodium interactions to affect the CO insertion rate. To provide further insight into the electronic and steric factors, and to quantify their relative importance, we studied in

† Electronic supplementary information (ESI) available: computed bonding energies and calculated atomic coordinates. See http://www.rsc.org/suppdata/dt/b2/b206610f/

DOI: 10.1039/b206610f

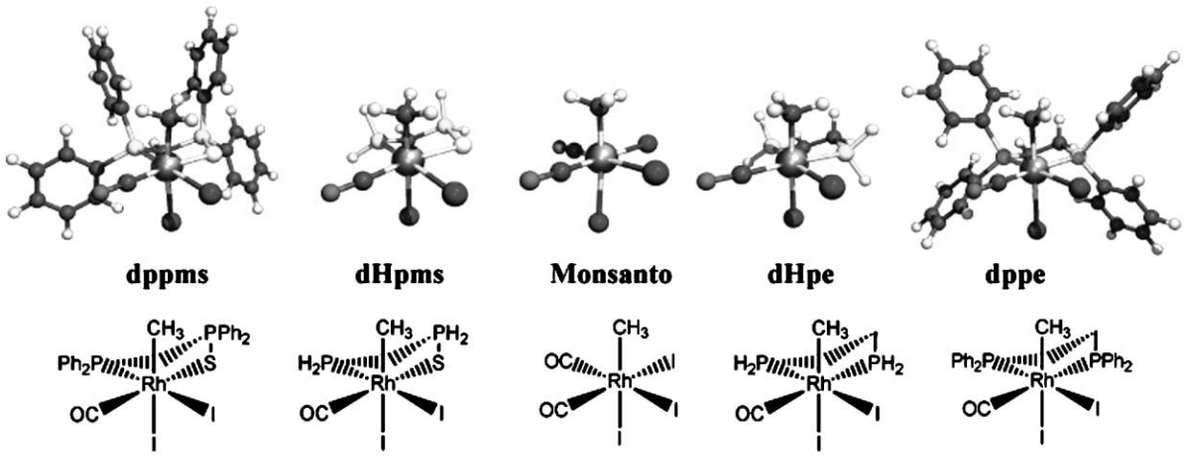

Fig. 1 Molecular structures of the octahedral complexes.

detail the migratory CO insertion step for the dppms and dppe systems, the Monsanto catalysts and several electronically unsymmetrical diphosphine model systems. We used DFT methods and QM/MM strategies, especially the IMOMM method[26,27] which has been proved very useful for analyzing similar questions in other systems.[28–30]

Recently, Cavallo and Solà[31] reported a comprehensive study of the MeI oxidative addition and the carbonyl insertion steps. They studied some of the bidentate ligands we did and used roughly the same method. The energy barriers they computed for the carbonyl insertion step[31] are in excellent agreement with kinetic data[17] for both dppms and dppe ligands. These authors reported that the relief in steric effects when the systems move from the reactants to the transition states is responsible for lowering the barrier. In our study we demonstrate that electronic effects may actually be more important and that previous interpretation may need reconsideration. We focus our report on two main topics: the origin of the difference between dppms and dppe, and the effect of phosphine basicity on different coordination sites.

Computational details

Stationary points on the potential energy surface were determined using the Amsterdam density functional program (ADFv1999), developed by Baerends *et al.*[32,33] The numerical integration scheme used in the calculations was developed by te Velde *et al.*,[34,35] and the geometry optimization algorithms were implemented by Versluis and Ziegler.[36] The electronic configurations of the molecular systems were described by a triple zeta plus polarization Slater type basis set. The 1s–3d electrons for Rh, the 1s–4d electrons for I, the 1s electrons for C and O and the 2p electrons for P and S were treated as frozen cores. Energy differences were calculated by augmenting the local VWN exchange-correlation potential with non-local Becke's exchange-correlation corrections[37] and Perdew's correlation corrections[38] (BP86). First-order Pauli scalar relativistic corrections were added variationally to the total energy for all systems. No symmetry constraints were used. Transition states for model systems were fully optimized with one imaginary frequency.

QM/MM calculations were carried out applying the IMOMM method[26] as implemented in the ADF package.[39] The QM level we used was the same as the one in the above paragraph. AMBER[40] or SYBYL[41] force fields were used as implemented in ADF to describe the atoms included in the MM part. For the rhodium atom, we used UFF parameters from the literature.[42] The ratio between the P–C bond distance and the P–H bond distance, taken from pure QM calculations was 1.296. This ratio is used to automatically position the atoms included in the MM part.

Results and discussion

dppms *vs.* dppe

We determined and characterized the structure of the reactants, transition states and products for the $RhMe(CO)I_2(L–L)$ (L–L = dppms and dppe) systems, and for the Monsanto complex $[RhMe(CO)_2(I)_3]^-$. Fig. 1 shows the molecular structures of the reactants and Table 1 collects some selected geometrical parameters for the reactants, TSs and products. We begin our discussion by considering the model systems in which phenyl phosphine substituents were replaced by hydrogen atoms, *i.e.* the $PH_2–CH_2–P(S)PH_2$ (dHpms) and $PH_2–CH_2CH_2–PH_2$ (dHpe) model ligands. In these model systems, there were no steric effects due to phenyls, only effects due to the electronic properties of P- and S-donor ligands. The most significant difference between the dHpe and dHpms octahedral complexes was in the rhodium carbonyl bonds, which were *trans* to a phosphine and phosphine sulfide ligand, respectively. Clearly, the shortest distance was for dHpms, since its π-donor ability promoted greater electron density on the metal and led to stronger M(d)⟶CO(π*) back-bonding. Transition state structures also reflected this trend. In the $[MeIr(CO)I_2(dppms)]$ complex, the angle P–Ir–Me was considered[17] as an indication of the steric hindrance induced by a phosphine phenyl on the methyl ligand (P–Ir–Me = 96.3°). The P–Rh–Me angles in Table 1 are 95.5 and 93.6° for dHpms and dHpe, respectively. This suggests that these angles do not indicate steric hindrance because the angle obtained with hydrogen atoms already reaches that value. This angle is higher in the TS structures for both the dHpe and the dHpms systems.

For these model systems, which lack any steric hindrance, the difference in the energy barriers for the carbonyl insertion of dHpms and dHpe ligands is already 16 kJ mol^{-1} (Table 2). At this level, the energy difference is somewhat lower than the difference in the experimental activation enthalpies (29 kJ mol^{-1}).[17] Fig. 2 shows a correlation diagram of the DFT molecular orbitals of dHpe, dHpms and the corresponding TSs. The graphs are designed so that the reader is watching the molecule from an Rh–I axis perpendicular to the plane of the paper. We found the eight p(π) iodide electrons located in the four MOs of highest energy, *i.e.*, the HOMO and the three levels below, which are well separated from the rest and maintain its energy in all cases. Fig. 2 clearly show that those eight electrons do not feel either the different P- or S- donating ligands or the methyl migration process. In dHpe, this is the second column in Fig. 2, the next two orbitals are mainly the other four p(σ) iodide electrons. The first, labeled as "p(σ)I(*y*)" in Fig. 2, is the anti-bonding combination of a iodide, methyl and a p rhodium orbital. The second, labeled as "p(σ) I(*z*)", is well localized on the other iodide. Then we found the three d metal orbitals (Rh(III)/d^6) labeled as d_{xy}, d_{yz} and d_{xz}. Those of

Table 1 Selected geometric parameters of reactants, TSs and products for dppms, dppe and Monsanto catalysts. Distances in Å and angles in degrees

Reactants	dppms	dppms (QM/MM)		dHpms	dHpe	dppe (QM/MM)		dppe	Monsanto
		SYBYL	AMBER			SYBYL	AMBER		
Rh–C(Me)	2.128	2.130	2.133	2.134	2.139	2.143	2.141	2.138	2.144
Rh–CO	1.862	1.853	1.853	1.856	1.904	1.898	1.899	1.890	1.874
C(Me)–CO	2.856	2.850	2.862	2.844	2.917	2.786	2.836	2.848	2.890
P–Rh–C(Me)	96.3	100.7	95.9	95.5	93.6	91.5	93.7	90.8	92.2
CO–Rh–C(Me)	91.1	91.0	91.5	90.6	92.1	86.9	88.9	89.7	91.7

Transition states	dppms	dppms(QM/MM)		dHpms	dHpe	dppe (QM/MM)		dppe	Monsanto
		SYBYL	AMBER			SYBYL	AMBER		
Rh–C(Me)	2.337	2.344	2.333	2.341	2.366	2.375	2.378	2.371	2.352
Rh–CO	1.840	1.855	1.847	1.854	1.900	1.893	1.898	1.888	1.872
C(Me)–CO	1.845	1.883	1.927	1.893	1.828	1.856	1.831	1.891	1.892
P–Rh–C(Me)	99.7	101.4	101.1	101.0	101	100.6	99.5	99.4	98.2
CO–Rh–C(Me)	50.7	51.6	53.3	52.1	49.2	49.9	49.1	51.1	51.7

Products		dppms	dppms(QM/MM)		dHpms	dHpe	dppe (QM/MM)		dppe	Monsanto
	X-Ray[a]		SYBYL	AMBER			SYBYL	AMBER		
Rh–C	1.95	1.977	1.987	1.991	1.987	1.997	1.998	1.998	1.993	2.008
Rh–P	2.26	2.282	2.242	2.238	2.234	2.257	2.255	2.261	2.292	(Rh–CO) 1.849
Rh–S	2.36	2.357	2.388	2.387	2.377	(Rh–P) 2.258	2.259	2.264	2.301	(Rh–I) 2.759
Rh–I (*trans* P)	2.70	2.782	2.744	2.746	2.753	2.748	2.751	2.750	2.771	2.752
Rh–I (*trans* S)	2.65	2.716	2.723	2.727	2.721	2.750	2.745	2.750	2.755	2.774
C(COMe)–Rh–P	92.8	91.6	90.4	92.0	88.8	90.0	90.4	92.0	90.4	93.6
C(COMe)–Rh–S	93.6	89.2	94.4	92.9	94.0	89.6	94.4	93.0	90.6	96.3
P–Rh–S	90.5	94.7	94.8	95.0	95.5	(P–Rh–P) 86.7	94.8	95.0	87.4	(CO–Rh–I) 86.6

[a] Ref. 17.

Table 2 Energy barriers ($\Delta E^{\neq}$) and reaction energies (ΔE_{react}) for dppms, dppe, dHpms, dHpe and the Monsanto catalyst. Values in kJ mol^{-1}

	QM		QM/MM		QM		QM
	dppms	dppe	dppms SYBYL (AMBER)	dppe SYBYL (AMBER)	dHpms	dHpe	Monsanto
$\Delta E^{\neq}$	66	78	73.5 (73)	86 (81.5)	75	91	79
ΔE_{reac}	−35.1	−56.4	−44 (−35.5)	−34 (−37)	−24	−24	−20

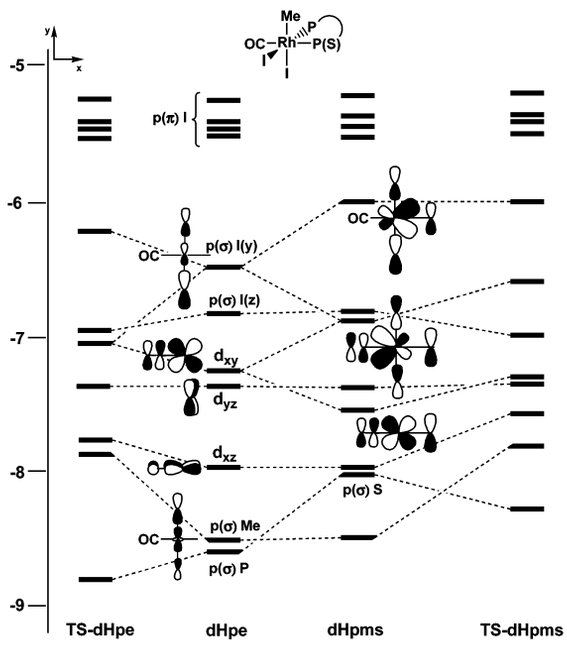

Fig. 2 Occupied molecular orbitals diagram of reactants and TSs for dHpms and dHpe. Energy scale in eV.

appropriate symmetry contribute to the d⟶CO(π*) back-bonding. Below the d metal levels we found the "methyl lone-pair" p(σ)Me as the bonding combination of methyl, iodide, and an empty d_{z^2} rhodium orbital, and the last one in Fig. 2, p(σ)P corresponds to the lone-pair of the phosphine *trans* to carbonyl.

When dHpe is substituted by dHpms, sulfur replaces the phosphine ligand and dramatic changes in the electronic structure are observed. A σ-donor/π-acceptor ligand provides two electrons whereas a σ-donor/-π-donor ligand provides four. Actually, the electronic structure of dHpms is best understood as the interaction of dHpe with a filled p(π) orbital. According to the axis convention in Fig. 2, a filled p_y orbital interacts with the p(σ)I(*y*) and with d_{xy}. These interactions produce three new d_{xy}-like molecular orbitals that are schematically shown in Fig. 2. All three are destabilized because the interaction between filled orbitals is repulsive. If we ignore the four p(π)I levels, the molecular orbital of highest energy in dHpms is above the corresponding level in dHpe. The enhanced back-bonding rhodium–carbonyl is clearly visualized in Fig. 2: the second d_{xy}-like MO presents the metal d lobes strongly polarized towards carbonyl. Interestingly, in that MO the contribution of the methyl ligand is not negligible and is in phase with metal and CO(π*), thus it generates a continuous lobe that contains the three atoms involved in migratory CO insertion. Note that the rhodium–sulfur bond order due to these π interactions is zero.

Due to symmetry, p(σ)Me and those dHpe orbitals which present a *z* component do not interact with sulfur, therefore such levels are degenerate in both complexes. Fig. 2 shows the evolution of the energy levels when the systems move to the TSs. In dHpe, there are four MOs involved in the migratory insertion, namely p(σ)I(*y*), d_{xy}, d_{xz} and p(σ)Me, that become destabilized in the TS, whereas the p(σ)P level is more stable. However, in dHpms there are five MOs involved: the highest one becomes more stable while the other four and the p(σ)S level, follow the same trend observed for dHpe.

The most significant point is that when the systems move to the transition state, molecular orbitals destabilize though not as much as with dHpms. Although the two additional electrons produce some destabilization in dHpms, they stabilize the TS. This analysis explains why the transition state is more stable in the dHpms system than it is in the dHpe system, and demonstrates that dHpms and dHpe exhibit different electronic features.

Experimentally tested ligands, dppe and dppms, were fully considered at QM/MM and QM levels of theory. Table 1 shows a selection of the geometrical parameters we obtained. Our values in Table 1 agree quite well with X-ray data for the penta-coordinated acyl dppms product complex.[17] The rhodium iodide bonds are the parameters that are the most different from the experimental values (0.06/0.08 Å). These results were slightly different from those recently obtained by other authors, whose parameters showed a larger discrepancy.[31] The lack of relativistic effects (specially for Rh and I) and a slightly smaller basis set could explain that discrepancy. We tested two force fields in the QM/MM calculations to assess their reliability. Table 1 shows that generally SYBYL and AMBER force fields produced almost identical structures, especially for products. The greatest differences were found in the reactive center, *i.e.* the rhodium, methyl and carbonyl framework, especially in the C(Me)–CO distance, which was slightly longer for AMBER than for SYBYL. In general, the geometric parameters obtained at the QM/MM level with the two force fields agree better with the values calculated at full QM level than with the geometries of the model systems. Differences in the force fields were quite small: 0.082 Å in the AMBER value for the C(Me)–CO bond in the dppms TS and 5° in the C(COMe)–Rh–S angle in the dppms product. Note that when we compare QM results for dppms and dppe, rhodium–methyl and rhodium–carbonyl bonds are significantly shorter for dppms in both the reactant and in the TSs due to the enhanced back-donation.

The geometry of the dppms complex agrees well with the X-Ray data for the iridium analog in ref. 17. In the computed structure, the conformation of the phenyls is fully equivalent to the X-ray disposition, even the close contact between hydrogens of the methyl and phenyl groups is well reproduced (X-Ray = 1.9 Å, computed = 2.09 Å). The five-membered chelate ring adopts an envelope conformation that places two phenyl groups in axial positions creating a crowded pocket surrounding the methyl group. In dppe, the same envelope conformation places one phenyl axial and one equatorial, although the frontal view in Fig. 1 erroneously suggests that the pocket is more crowed in dppms than it is in dppe. In dppms, the two phenyl groups lie almost parallel, due to a putative face-to-face π stacking. Therefore, one phenyl group is relatively close to methyl, with the shortest distance between the methyl carbon atom and a phenyl carbon being 3.75 Å. However, the other phenyl is more distal with the shortest distance between hydrogens of the methyl and the other phenyl group being 2.65 Å, and the shortest distance between the methyl carbon atom and a phenyl carbon is 4.09 Å. In dppe, the two phenyl groups does not experiment π stacking, and both are relatively close to methyl. The shortest distances between the methyl carbon atom and phenyl carbon atoms are

Table 3 Selected geometric parameters of reactants and TSs for model phosphines, relative stability of the different isomers and energy barriers for the migratory CO insertion step. Distances in Å, angles in ° and energies in kJ mol^{-1}

	PF_2–PF_2 L1	PMe_2–PF_2 L2	PH_2–PF_2 L3	PF_2–PH_2 L3′	PH_2–PH_2 L4	PF_2–PMe_2 L2′	PMe_2–PH_2 L5	PMe_2–PMe_2 L6	PH_2–PMe_2 L5′
Reactants									
Rh–C(Me)	2.153	2.148	2.147	2.148	2.139	2.146	2.139	2.138	2.139
Rh–CO	1.931	1.914	1.922	1.92	1.904	1.923	1.901	1.904	1.913
C(Me)–CO	2.858	2.846	2.880	2.885	2.917	2.888	2.868	2.886	2.896
P1–Rh–C(Me)	96.6	95.3	94.7	96.4	93.6	95.7	95.1	94.3	93
CO–Rh–C(Me)	88.6	88.7	89.9	90.1	92.1	90.2	90.2	90.9	91
Relative stability[a]	—	21.3	19.6	0	—	0	3.7	—	0
Transition states									
Rh–C(Me)	2.369	2.371	2.365	2.371	2.366	2.383	2.373	2.379	2.375
Rh–CO	1.921	1.908	1.912	1.908	1.899	1.912	1.895	1.902	1.906
C(Me)–CO	1.843	1.833	1.834	1.837	1.828	1.835	1.822	1.805	1.811
P1–Rh–C(Me)	101.1	99.2	99.8	101.5	101.1	100.7	99.6	99.1	100.1
CO–Rh–C(Me)	49.5	49.2	49.4	49.4	49.2	49.1	48.9	48.3	48.5
Energy barrier	81.9	82.7	83.6	88.6	90.7	91.1	91.5	94.0	96.5

[a] Note that empty cells correspond to electronically symmetric diphosphines.

3.37 and 3.25 Å. The shortest distance between hydrogens of the methyl and the phenyl groups are 2.28 and 2.59 Å. Therefore, this comparative analysis of the geometry of dppms and dppe complexes suggests that the two phenyl groups in dppms are close to the methyl though not as close as in dppe.

The IMOMM method used in this paper relies on an additive scheme to obtain the total energy of a molecular system as the sum of QM and MM contributions. By comparing energetic data at different levels for different model systems, we can separate electronic and steric effects and evaluate their relative importance.[28,29] This kind of analysis depends strongly on the choice of the model, *i.e.* on the division in atoms treated at the QM level and those treated at the MM level. In our study, the reactive center, iodide ligands and diphosphine backbone were fully treated at the QM level but only phenylphosphine substituents are included in the MM part. In this way, the QM/MM calculations incorporated only what could be considered as steric effects due to the phenyl substituents, since the QM part includes phosphines whose hydrogen atoms replace phenyl groups, as occurs in the model systems. We needed to include phenyl groups in the QM part to account for electronic effects due to phosphine basicity. If we compare full QM with QM/MM data, we can analyze and evaluate the electronic contributions. Table 2 shows that the steric effects introduced by the QM/MM calculations lowered the energy barrier, more than in the model systems. For dppms, both force fields lowered the barrier by 2 kJ mol^{-1}, whereas for dppe the AMBER and SYBYL values were 9 and 5 kJ mol^{-1}, respectively. If we split the QM/MM energy barrier into its constituent parts ($\Delta E^{\neq}_{QM}$ + $\Delta E^{\neq}_{MM}$), we can see that for both force fields, the MM contribution with dppe was greater than it was with dppms. This means that the reduction in steric hindrance when the systems moved to the transition states was larger for dppe than it was for dppms, given that individual MM contributions were positive in all cases and that the greatest individual contribution was made by the dppe reactant. Moreover, steric effects reduced the dppe energy barrier more because the phenyl substituents induced more steric hindrance with dppe than with dppms. This proves that dppe ligand generates more steric hindrance than dppms, and that the reduction in steric congestion in the TS is therefore larger for dppe than for dppms. This result is in line with those reported in ref. 31 although those authors did not comment on this.

When we treated dppms and dppe complexes at full QM level, the energy barriers were even smaller. In this case, the lowering of the barriers was due to both electronic and steric effects generated by phenylphosphino substituents. If we compare the results at full QM level to the results for the model systems, energy barriers were reduced by 9 and by 13 kJ mol^{-1} for dppms and dppe, respectively. If we compare these results with those from QM/MM, we can see that for dppms the electronic contribution was much larger than the steric contribution: the electronic contribution to barrier lowering was 78% whereas the steric contribution was 22%. For dppe, as we saw above, the steric effects were larger because two phosphines were coordinated to rhodium and phenyls are closer to methyl (Fig. 1). The two force fields we tested gave different results (38% SYBYL, 73% AMBER), but in both cases the values were larger than those for dppms.

At the full QM level, the difference in the energy barriers of the dppms and dppe systems was 12 kJ mol^{-1}, which is lower than the value reported. Absolute values[17] are 54 ± 7 and 83 ± 2 kJ mol^{-1} for dppms and dppe, respectively, while our values were 66 and 78 kJ mol^{-1}, and those of Cavallo and Solà were 56 and 61 kJ mol^{-1}, respectively. Theoretical determination of absolute energy barriers for these kinds of systems challenges theoretical methods, since it requires proper evaluation of all energy components (zero point energy and entropic contributions) for reactants and TSs and the proper inclusion of solvent effects. These tasks are beyond the scope of current computational resources. In any case, the agreement between the measured and the calculated values can be considered excellent. Both theoretical studies predict that the dppms system reacts faster than the dppe system, although they also underestimate the barrier for dppe.

Electronically unsymmetrical diphosphines

To systematically study the influence of phosphine basicity in the energy barrier of the CO migratory insertion, we considered a set of model diphosphines. We kept the diphosphine backbone $X_2PCH_2CH_2PX_2$, and considered all possible combinations of F, H and Me substituents in X_2 positions, *i.e.* F_2P–PF_2, H_2P–PH_2 and Me_2P–PMe_2, and the asymmetric complexes of H_2P–PF_2, Me_2P–PF_2 and Me_2P–PH_2. As Woska *et al.*[43] recently reported, these three substituents (F, H and Me) cover the full range of electronic properties of phosphines. PF_3 is the poorest σ-donor and the strongest π-acid phosphine, PMe_3 is the strongest σ-donor and the poorest π-acid, and PH_3 is in an intermediate situation being more similar to PMe_3 than to PF_3. On this scale, PPh_3 lies between PMe_3 and PH_3.

Reactant and transition state structures were determined at the QM level (see Table 3). A good correlation was found for Rh–CO and Rh–Me bond distances with phosphine basicity: both bond distances increased when phosphine basicity decreased in the order F ≫ H > Me. Among the series, the Rh–CO bond changed more than the Rh–Me bond, but following the same tendency. Each unsymmetrical diphosphine had

two isomers. We denoted by $X_2P–PY_2$ the complex where the PX_2 and PY_2 moieties are *cis* and *trans* to carbonyl, respectively. The stability of $PH_2–PMe_2$ and $PMe_2–PH_2$ was similar (Table 3). $PH_2–PMe_2$ was the most stable isomer (3.7 kJ mol^{-1} more stable than $PMe_2–PH_2$). The $PF_2–PH_2$ isomer was 19.6 kJ mol^{-1} more stable than $PH_2–PF_2$ and $PF_2–PMe_2$ was 21 kJ mol^{-1} more stable than $PMe_2–PF_2$. In all cases, the preferred isomer presented the least basic phosphine *trans* to iodide, since this strong donor ligand stabilized its *trans* π-acceptor ligand.

There was a smooth variation of about 15 kJ mol^{-1} in energy barriers and the lowest value corresponded to the least basic diphosphine. This result agrees with the fact that the strong electron-withdrawing power of the F substituents in *trans* and *cis* position relative to CO helps to elongate of Rh–Me and Rh–CO bonds. We can see this observation in other cases too. An electron-withdrawing substituent *trans* to CO reduced the activation barrier in the order: F < H < Me. The energy barrier in PF_2 groups was lower than in the model system $PH_2–PH_2$, except for the Me group *trans* to CO, whose energy barrier always increased. The substituents *cis* to CO did not have such a great effect. When a PF_2 group was *trans* to CO, the energy barrier changed slightly for PF_2, PMe_2 or PH_2. Even the least basic diphosphine $F_2P–PF_2$ did not reach the low energy barrier of the dppe system. If we consider only electronic properties we should expect a PPh_2 group to behave half way between H and Me.[43] However, as we discussed above, the bulkiness of the phenyl groups is also an important factor behind the lower energy barrier in the dppe system.

Finally, let us consider the relative stability of unsymmetrical diphosphine complexes and their reactivity. Table 3 shows that in all three cases, the most stable isomer was the least reactive one. This was because phosphine basicity affected stability and reactivity in opposite ways. The least basic phosphine moiety prefered a coordination mode *trans* to iodide, but the reaction was accelerated when the least basic phosphine was *trans* to CO. The more electronically different the ligands are, the greater the difference in stability and in reactivity.

Conclusions

Using DFT calculations and QM/MM strategies, we studied how electronic and steric properties of a variety of ligands determine the energy barrier of the migratory carbonyl insertion in complexes $RhMe(CO)I_2(L–L)$. The agreement between the calculated energy barriers and the activation energies for dppms and dppe systems was excellent. The difference between the reaction rates of dppms and dppe has a clear electronic origin that reflects the different properties of sulfide phosphine (π-donor) ligands and phosphine (π-acid) ligands. Molecular orbitals clearly show that dppms strongly increases the degree of back-bonding to CO and favours the overlap between CO and methyl. These are factors that facilitate the reaction. Steric effects modulate the barrier and contribute to decreasing it more for dppe than for dppms. For dppms, the contribution to lowering the barrier made by the electronic effects of phenylphosphine substituents is greater than the contribution made by purely steric effects. The sulfide phosphine ligand dppms accelerates carbonyl insertion because its π-donor capability. This conclusion seems to contradict the belief that electron-donating ligands retard CO insertion.

Effectively, the energy barrier of the model diphosphine ligands we studied varied gradually as basicity varied, and the complex contaning the most electron-donating phosphine reacts more slowly. This effect is stronger when phosphine basicity is varied in *trans* position to CO. Thus, the apparent contradiction vanishes if we realize that we cannot extrapolate the behaviour of a π-acceptor ligand to that of a π-donor ligand. The MO analysis present above demonstrates that the electronic structures of dppms and dppe are different. Thus, the above mentioned rule certainly remains valid if it is applied to a similar kind of electron-donating ligands, though not to dppe and dppms.

On the other hand, poor electron-donating ligands are preferred in *cis* position because of the stability of electronically unsymmetrical diphosphines. The more different the two moieties, the greater the difference in stability. In all cases, the three phosphine substituents followed the order F ⩾ H > Me.

We believe that these conclusions are general enough to suggest ways of designing faster catalysts for the carbonyl insertion step. Despite the greater reactivity observed using the dppms system, diphosphines are preferred due to catalyst stability.[24,25] Electron-withdrawing phenyl substituents would reduce phenylphosphine basicity and mantain steric hindrance (*e.g.* p-C_6H_4F or p-$C_6H_4CF_3$ groups). Phosphite ligands, though less basic and less bulky, should produce faster catalysts. Electronically unsymmetrical ligands are of less interest because the factors that favor stability hinder reactivity. Since these kinds of ligands may be interesting in terms of asymmetric induction, we recommend using electronically equivalent but sterically different diphosphines. Since the angle P–Rh–P changes slightly to reach the TS (about 90°), using wider bite angle diphosphines would not be a significant factor.

Acknowledgements

We gratefully acknowledge financial support from the Spanish DGICYT under Project PB98–0916–C02–02, and from the CIRIT of the Generalitat de Catalunya under Project SGR-1999–00182. We thank the referees for insightful suggestions, Prof. L. Cavallo and Prof. M. Solá for helpful comments, and José C. Ortiz for technical assistance.

References

1 (*a*) M. Gauss, A. Seidel, P. Torrence, and P. Heymans, *Applied Homogeneous Catalysis with Organometallic Compunds*, ed. B. Cornils, and W. A. Herrmann, VCH, New York, 1996; (*b*) M. J. Howard, M. D. Jones, M. S. Roberts and S. A. Taylor, *Catal. Today*, 1993, **18**, 325.
2 D. Forster, *J. Am. Chem. Soc.*, 1976, **98**, 846.
3 D. Forster, *Adv. Organomet. Chem.*, 1979, **17**, 255.
4 S. B. Dake and R. V. Chaudhari, *J. Mol. Catal.*, 1984, **26**, 135.
5 A. Haynes, B. E. Mann, G. E. Morris and P. M. Maitlis, *J. Am. Chem. Soc.*, 1993, **115**, 4093.
6 T. R. Griffin, D. B. Cook, A. Haynes, J. M. Pearson, D. Monti and G. E. Morris, *J. Am. Chem. Soc.*, 1996, **118**, 3029.
7 T. Ghaffar, H. Adams, P. M. Maitlis, G. J. Sunley, M. J. Baker and A. Haynes, *Chem. Commun.*, 1998, 1359.
8 M. Cheong, R. Schmid and T. Ziegler, *Organometallics*, 2000, **19**, 1973.
9 E. A. Ivanova, P. Gisdakis, V. A. Nasluzov, A. V. Rubailo and N. Rösch, *Organometallics*, 2001, **20**, 1161.
10 T. Kinnunen and K. Laasonen, *J. Mol. Struct. (THEOCHEM)*, 2001, **540**, 91.
11 T. Kinnunen and K. Laasonen, *J. Mol. Struct. (THEOCHEM)*, 2001, **542**, 273.
12 T. Kinnunen and K. Laasonen, *J. Organomet. Chem.*, 2001, **628**, 222.
13 J. Rankin, A. C. Benyei, A. D. Poole and D. J. Cole-Hamilton, *J. Chem. Soc., Dalton Trans.*, 1999, 3771.
14 K. G. Moloy and R. W. Wegman, *Organometallics*, 1989, **8**, 2889.
15 R. W. Wegman, *Chem. Abstr.*, 1986, **105**, 78526g.
16 M. J. Baker, M. G. Giles, A. G. Orpen, M. J. Taylor and R. J. Watt, *J. Chem. Soc., Chem. Commun.*, 1995, 197.
17 L. Gonsalvi, H. Adams, G. J. Sunley, E. Ditzel and A. Haynes, *J. Am. Chem. Soc.*, 1999, **121**, 11233.
18 H.-S. Lee, J.-Y. Bae, D.-H. Kim, H. S. Kim, S.-J. Kim, S. Cho, J. Ko and S. O. Kang, *Organometallics*, 2002, **21**, 210–219.
19 K. V. Katti, B. D. Santarsiero, A. A. Pinkerton and R. G. Cavell, *Inorg. Chem.*, 1993, **32**, 5919.
20 C. A. Carraz, E. J. Ditzel, A. G. Orpen, D. D. Ellis, P. G. Pringle and G. J. Sunley, *Chem. Commun.*, 2000, 1277–1278.
21 R. W. Wegman, A. G. Abatjoglou and A. M. Harrison, *J. Chem. Soc., Chem. Commun.*, 1987, 1891.
22 A. Bader and E. Lindner, *Coord. Chem. Rev.*, 1991, **108**, 27.
23 M. S. Balakrishna, R. Klein, S. Uhlenbrock, A. A. Pinkerton and R. A. Cavell, *Inorg. Chem.*, 1993, **32**, 5676.

24 M. J. Baker, M. G. Gile, A. G. Orpen, J. Taylor and R. J. Watt, *J. Chem. Soc., Chem. Commun.*, 1995, 197.
25 J. R. Dilworth, J. R. Miller, N. Wheatley, M. J. Baker and G. Sunley, *J. Chem. Soc., Chem. Commun.*, 1995, 1579.
26 F. Maseras and K. Morokuma, *J. Comput. Chem.*, 1995, **16**, 1170.
27 F. Maseras, *Chem. Commun.*, 2000, 1821–1827.
28 G. Ujaque, F. Maseras and A. Lledós, *J. Am. Chem. Soc.*, 1999, **121**, 1317.
29 J. J. Carbó, F. Maseras, C. Bo and P.W.N.M. van Leeuwen, *J. Am. Chem. Soc.*, 2001, **123**, 7630.
30 H. Jacobsen and L. Cavallo, *Chem. Eur. J.*, 2001, **7**, 800.
31 L. Cavallo and M. Solà, *J. Am. Chem. Soc.*, 2001, **123**, 12294–12302.
32 E. J. Baerends, D. E. Ellis and P. Ros, *Chem.Phys.*, 1973, **2**, 41.
33 C. Fonseca Guerra, J. G. Snijders, G. te Velde and E. J. Baerends, *Theor. Chem. Acc.*, 1998, **99**, 391.
34 G. te Velde and E. J. Baerends, *J. Comput. Chem.*, 1992, **99**, 84.
35 P. M. Boerrigter, G. t. Velde and E. J. Baerends, *Int. J. Quantum Chem.*, 1988, **33**, 87.
36 L. Versluis and T. Ziegler, *J. Chem. Phys.*, 1988, **88**, 322.
37 A. Becke, *Phys. Rev. A*, 1988, **38**, 3098.
38 (*a*) J. P. Perdew, *Phys Rev. B.*, 1986, **34**, 7406; (*b*) J. P. Perdew, *Phys Rev. B.*, 1986, **33**, 8822.
39 T. K. Woo, L. Cavallo and T. Ziegler, *Theor. Chem. Acc.*, 1998, **100**, 307.
40 W. D. Cornell, P. Cieplak, C. I. Bayly, I. R. Gould, K. M. Merz, Jr., D. M. Ferguson, D. C. Spellmeyer, T. Fox, J. W. Caldwell and P. A. Kollman, *J. Am. Chem. Soc.*, 1995, **117**, 5179–5197.
41 (*a*) M. Clark, R. D. Cramer III and N. van Opdenbosch, *J. Comput. Chem.*, 1989, **10**, 982–1012; (*b*) U. C. Singh and P. A. Kollman, *J. Comput. Chem.*, 1986, **7**, 718–730.
42 A. K. Rappé, C. J. Casewit, K. S. Colwell, W. A. Goddard III and W. M. Shiff, *J. Am. Chem. Soc.*, 1992, **114**, 10024.
43 D. Woska, A. Prock and W. P. Giering, *Organometallics*, 2000, **19**, 4629.